A Journal of the Gesellschaft Deutscher Chemiker

Angewandte Chemie

International Edition

www.angewandte.org

Accepted Article

Title: Evidence for Methylaluminoxane (MAO) Molecular Structure and Reactivity from Ultra-High Magnetic Field 27Al MAS NMR Spectroscopy Combined with DFT Calculations.

Authors: Kai C. Szeto, Mostafa TAOUFIK, Franck Fayon, David Gajan, Eva Zurek, Jochen Autschbach, Julien Trebosc, Laurent Delevoye, and Régis Michaël Gauvin

To be cited as: *Angew. Chem. Int. Ed.* **2025**, e202508409

Link to VoR: https://doi.org/10.1002/anie.202508409

WILEY-VCH

Evidence for Methylaluminoxane (MAO) Molecular Structure and Reactivity from Ultra-High Magnetic Field ^{27}Al MAS NMR Spectroscopy Combined with DFT Calculations.

Kai Szeto,[a] Mostafa Taoufik,*[a] Franck Fayon,[b] David Gajan,[c],Eva Zurek,[d] Jochen Autschbach,*[d] Julien Trébosc,[e], Laurent Delevoye,*[e] and Régis M. Gauvin*[f]

Dedicated to the memory of Prof. W. Kaminsky, the inventor of MAO, who passed away in November 2024.

[a] Dr K. Szeto, Dr. M. Taoufik
Univ. Lyon 1, CPE Lyon, CNRS UMR 5128, Laboratoire de Catalyse Polymérisation Procédés et Matériaux (CP2M), Université de Lyon, F-69616 Villeurbanne, France
E-mail: mostafa.taoufik@univ-lyon1.fr

[b] Dr. F. Fayon
CNRS, CEMHTI UPR3079, Univ. Orléans, Orléans F-45071, France

[c] Dr. D. Gajan
Centre de RMN à Hauts Champs de Lyon CRMN, UMR5082, Université de Lyon, CNRS, ENS Lyon (France)
Current affiliation: Centre de Spectrométrie de La Doua, C-SPEC LaDoua, CNRS, F-69616 Villeurbanne, France and same as [b]

[d] Prof. E. Zurek, Prof. J. Autschbach
Department of Chemistry
University at Buffalo, State University of New York
Buffalo, New York, 14260-3000, USA
E-mail: jochena@buffalo.edu

[e] Dr. J. Trébosc
Univ. Lille, CNRS, INRAE, Centrale Lille, Univ. Artois, FR 2638 – IMEC – Fédération Chevreul F-59000, Lille, France

[f] Dr. L. Delevoye
Univ. Lille, CNRS, Centrale Lille, Univ. Artois, UMR 8181, UCCS, Unité de Catalyse et Chimie du Solide
59000 Lille, France
E-mail: Laurent.delevoye@univ-lille.fr

[g] Dr. R. M. Gauvin
Chimie ParisTech, PSL University, CNRS, Institut de Recherche de Chimie Paris
11, rue Pierre et Marie Curie, 75005 Paris, France
E-mail: regis.gauvin@chimieparistech.psl.eu

Supporting information for this article is given via a link at the end of the document.

Abstract: The structure and reactivity of methylaluminoxane (MAO), a reagent of major interest for olefin polymerization, both industrially and academically, has been probed using ultra-high magnetic field solid-state NMR (28.2 T, 1200 MHz for ^{1}H Larmor frequency). High resolution methods combined with density functional calculations allowed for the identification and quantification of five major aluminum sites, providing precise information on the structure of MAO at the molecular level. Based on reactivity studies with THF and [ZrCp$_2$Me$_2$], the main reactive centers are identified as bismethyl aluminum species stabilized via a bridging methyl group from a neighboring Al center, featuring both high chemical shift and quadrupolar coupling constants (162 ppm and 27.4 MHz, respectively). The approach demonstrates the ability to monitor the chemistry of MAO with unprecedented precision, enabling a state-of-the-art understanding of its structure and reactivity.

Introduction

Organoaluminum compounds are key industrial reagents, with consumption reaching hundreds of thousands of tons per year for stoichiometric and catalytic reactions.[1] Among them, methylaluminoxane (MAO, whose simplified formula is often given as $[AlOMe)_n]$ holds a specific position. Following its serendipitous discovery by Kaminsky and coworkers, MAO triggered a major breakthrough in the field of olefin (co)polymerization, enabling unprecedented activity levels when used as an activator for metallocene and post-metallocene pre-catalysts. MAO has contributed to the industrial production of polyolefins with a high degree of control over composition, microstructure, and mass distribution.[2] The major roles of MAO in these processes are well established: it acts as an alkylating agent for chloride precursors, an activator capable of generating catalytically active cationic alkyl species, and a scavenger for impurities within the reaction mixture. Even so, despite innumerable studies MAO remains shrouded in mystery.[3] For instance, mass spectrometry has revealed that MAO is composed of a broad variety of aluminum clusters, so its formula is better approximated as $[(AlOMe)_x(AlMe_3)_y]$, differing from the aforementioned idealized [AlOMe] stoichiometry.[4-7] These clusters exhibit molecular masses ranging from 1—2 kg mol^{-1}, corresponding to structures containing about 15 to 30 aluminum centers. The structure of MAO at the molecular level, which is intimately linked to its reactivity, remains unknown, which is a major hindrance for understanding and improving this key reagent. Indeed, the structural chemistry of aluminum alkyl derivatives is known to be rich and versatile. Replacement of methyl with the bulkier *tert*-butyl group, which prevented oligimerization, made the first structural determination of alkylaluminoxanes possible.[5,6] The ensuing oligomerization complicates the nature and distribution of the molecular entities constituting MAO. Theoretical calculations have significantly helped to put forward plausible molecular models for MAO. It has been proposed that the species comprising MAO can be described either as cage-like, or nano-tubular compounds, where methyl and oxide groups are redistributed among predominantly tetracoordinated aluminum centers.[8-11] Quantum chemical calculations revealed a variety of aluminum environments, including monomethyl aluminum species ($[O_3AlMe]$), bis-methyl species ($[O_2AlMe_2]$), along with complexed trimethyl aluminum (TMA), which is often located at the edges of the structures for stabilization. These TMA adducts form binuclear sites, where a trigonal $[OAlMe_2]$ is stabilized by a neighboring $[O_2AlXMe]$ (X=O, Me) via a bridging methyl group. The reactivity of MAO towards metallocenes, generating highly active olefin polymerization catalysts, is attributed to its potential to mediate the formation of an outer sphere metal alkyl ion pair, via a series of intricate exchanges between various species (Scheme 1). The main activation pathways include methide abstraction or activation via the $[AlMe_2]^+$ cation, leading ultimately to the catalytically active species.[12,13]

The role of TMA in MAO has long been recognized as crucial, influencing the catalytic reactivity of MAO-based systems either positively or negatively. Notably, Busico and coworkers pioneered the use of TMA-depleted MAO as a cocatalyst, exploiting the specific reactivity of complexed TMA towards sterically encumbered phenols.[14] Recently, the same group used density functional theory (DFT) calculations to study TMA-depleted MAO.[15] Focusing on the cluster proposed to be the most abundant $[(AlOMe)_{16}(AlMe_3)_6]$, they investigated the nature of sites prone to releasing activating $[AlMe_2]^+$ cations. Three types of Lewis acidic sites were identified, with only one capable of releasing $AlMe_3$ upon drying *in vacuo*. These studies thus provide clues on what may be the main structural features of MAO, awaiting experimental validation.

Further structural insights have emerged from recent experimental work. Luo et al. reported a single crystal X-ray diffraction study of a MAO component, revealing a sheet-like structure with the molecular formula $[(AlOMe)_{26}(AlMe_3)_9]$. This structure is composed of the same motifs as those predicted by DFT calculations. [16] Crucially, while the core of the structure is composed of monomethyl Al centers, it bears peripheral sites that formally result from $AlMe_3$ complexation. According to DFT predictions, some of these sites would readily release $[AlMe_2]^+$ upon reaction with THF.

Though numerous computational models have been proposed for the structures that might constitute MAO, experimental evidence has been limited to electro-spray ionization mass spectrometry and XRD. However, such experiments do not directly probe the molecular systems that are found within MAO. What is urgently required is an in situ method that does not perturb the chemical species. Moreover, when considering activation chemistry (Scheme 1), while metallocene-containing fragments have been identified and can be spectroscopically monitored, and besides Barron's model compounds,[6,17] there is no molecular description of the MAO reagent/counter anion within such systems because of the limitations of current analytical tools.

10.1002/anie.202508409

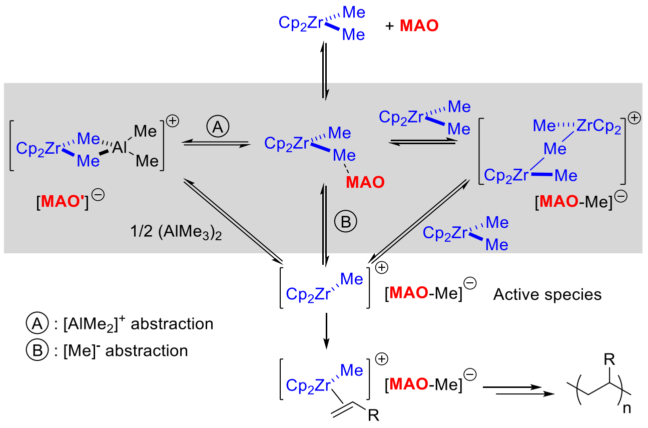

Scheme 1. Simplified pathways leading from $[ZrCp_2Me_2]$ to the polymerization active species. The gray background marks the equilibria occurring prior to active species generation.

Spectroscopic breakthroughs are still required to achieve a true understanding of MAO's structure and reactivity. NMR is an obvious choice because of its sensitivity to *local* structural features and non-invasive nature. While ^1H and ^{13}C nuclei have been extensively used to investigate MAO reactivity, only limited structural information has been gathered.[6,7,18,19] Conversely, ^{27}Al, a quadrupolar nucleus with I=5/2, offers significant potential for structural investigations, thanks to its wide chemical shift (CS) range, from 0 to about 200 ppm, which depends on the composition and geometry of the aluminum coordination sphere. In solution, ^{27}Al NMR spectra of MAO are typically unresolved or uninformative. However, in solid state NMR, anisotropic interactions, characterized by parameters such as the quadrupolar coupling constant (C_Q) and the asymmetry parameter (η_Q), offer additional structure-specific insights. These parameters can also be computed reliably using DFT, making ^{27}Al MAS NMR a highly promising approach for joint experimental/theoretical investigations of MAO.[20] So far, however, such efforts have faced significant challenges. Previous attempts, including by us, were thwarted by technical limitations, primarily, insufficient magnetic field strength.[21,22] However, as demonstrated in this study, the combination of ultra-high magnetic fields and high sample spinning frequencies provides an unprecedented, detailed view of the molecular structure of MAO by enabling the efficient recording of high-resolution data such as using Multiple-Quantum Magic-Angle Spinning (MQMAS) NMR method.

Herein, we first describe the main structural features of MAO models according to DFT calculations and provide their calculated ^{27}Al NMR parameters. Given that MAO consists of a mixture of clusters, we emphasize general trends rather than focusing on a specific MAO model. Since NMR provides information about local topology, the analysis prioritizes the first coordination spheres around the aluminum centers, which are largely unaffected by the long-range organization within the clusters. Subsequently, we compare these predicted values with experimental data, to establish a precise structural depiction of MAO. Additional insights will be gained by examining the reactivity of MAO with a Lewis base (THF) and a polymerization pre-catalyst ($[ZrCp_2Me_2]$).

Results and Discussion

MAO Models, Calculated NMR Parameter, and Ultra-High Field NMR Investigations

The models employed in the DFT calculations performed for this work are based on two types of structures proposed in previous theoretical investigations. The first is $[(AlOMe)_{16}(AlMe_3)_4]$, which represents MAO after "labile" TMA has been removed via vacuum drying, as described by Ehm and coworkers.[15] This corresponds to the cage structure **MAO-c-DFT** (Figure 1a). The second model is based on the sheet-like structure $[(AlOMe)_{26}(AlMe_3)_9]$, derived from the recent X-ray diffraction study (**MAO-s-DFT**, Figure 1b).[10]

Both structures feature similar classes of Al sites, labeled as $\mathbf{A_n}$, $\mathbf{B_n}$ and **C**, corresponding to mono-, bis-, and tris-alkyl coordination spheres, respectively (Figure 2a). The main component of MAO is $[AlO_3Me]$ ($\mathbf{A_1}$ and $\mathbf{A_2}$), which constitutes the backbone of the clusters and represents about half of the aluminum sites in both models. $\mathbf{A_2}$ differs from $\mathbf{A_1}$ in that one of its O-Al-O fragments is part of a strained 4-membered ring. In addition, the less abundant $[AlO_2Me_2]$ ($\mathbf{B_1}$) groups account for 11 and 15% of the sites in the cage and sheet models, respectively. At the periphery, several TMA-adducts" are present, including $[(O_2AlMe)(\mu\text{-}Me)(OAlMe_2)]$ sites (sites $\mathbf{B_2}$ and **C**, see Figure 2b for an example). In the **MAO-c-DFT** model, two extracted $AlMe_3$ molecules were originally bound to $[OAlMe_2]$ sites via bridging methyl groups, *i.e.* in the form $[OAlMe(\mu\text{-}Me)_2AlMe_2]$. The removal of these $AlMe_3$ units results in the formation of formally trigonal $[OAlMe_2]$ sites. In the DFT optimized **MAO-c-DFT** structure, one of these $[OAlMe_2]$ sites is stabilized via a long-range interaction with a methyl group from a neighboring $[AlO_3Me]$ moiety, resulting in a slightly distorted geometry. Such a trigonal configuration was previously proposed in a molecular model for MAO.[23]

Calculations were performed with the Amsterdam Density Functional (ADF) program and the accompanying NMR utility code[24,25] included in the Amsterdam Modeling Suite (AMS) version 2023.104.[26] Kohn-Sham DFT calculations of NMR parameters closely followed a previous study where the computational protocol was extensively benchmarked.[20] DFT calculations were performed with the revised PBE functional (revPBE),[27,28] D3 dispersion corrections for the geometry optimizations, triple-zeta

10.1002/anie.202508409

polarized (TZP) Slater-type atomic orbital (AO) basis sets from the ADF basis set library for non-hydrogen atoms, a double-zeta non-polarized (DZ) Slater-type basis for hydrogens, and the scalar zeroth-order regular approximation (ZORA) Hamiltonian. The TZP/DZ(H) basis set was chosen after running tests with some of the systems from the previous study[20] (the TMA dimer and the system in Figure 6 of the cited publication), which showed that polarization functions for hydrogens did not materially affect the calculated chemical shifts, quadrupole coupling constants, or optimized geometries.

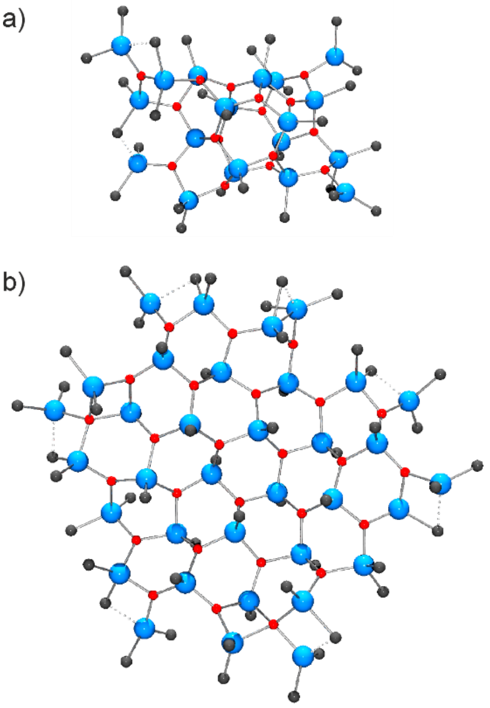

Figure 1. DFT-optimized MAO models for NMR parameter calculations: a) $[(AlOMe)_{16}(AlMe_3)_4]$ cage-type structure **MAO-c-DFT** and b) $[(AlOMe)_{26}(AlMe_3)_9]$ sheet-type structure **MAO-s-DFT**. H atoms omitted for clarity.

As illustrated in Figure 2c and summarized in Table 1, the DFT-calculated NMR parameters for the Al centers highlight distinct trends for the different site classes. The **A$_1$** and **A$_2$** sites, which form the backbone of the cluster, possess similar chemical shifts (CS) around 100 ppm but differ in quadrupolar coupling constants (C_Q) and asymmetry parameters (η_Q). Sites at the periphery, including **B$_1$**, **B$_2$**, and **C**, exhibit progressively higher CS and C_Q values. The $[OAlMe_2]$ sites feature the highest CS (~200 ppm, Fig. 2c) and C_Q values, reflecting their unique coordination environments. Interestingly, the interaction within the **B$_2$-C** fragments significantly decreases both the CS and C_Q values compared to the parent (non-interacting) **B$_1$** and $[OAlMe_2]$ sites.[29]

Table 1. NMR parameters of the main sites in MAO and related materials.

	Site	CS (ppm)[c]	C_Q (MHz)	η_Q	mol%[a]
MAO-1[b]	**A$_1$**	110.9 (98.8)	15.7 (16.7)	0.30 (0.25)	38 (44)
	A$_2$	120.0 (101.0)	18.9 (20.2)	0.45 (0.57)	7 (8)
	B$_1$	146.8 (150.7)	18.5 (23.8)	0.81 (0.76)	10 (13)
	B$_2$	124.0 (119.0)	19.0 (17.7)	0.45 (0.49)	21 (17)
	C	162.4 (162.3)	27.4 (28.9)	0.85 (0.89)	24 (17)
MAO-2	**A$_1$**	109.5	14.2	0.20	41
	A$_2$	117.1	18.8	0.45	6
	A$_3$	109.0	16.5	0.90	17
	B$_1$	141.0	16.6	0.80	19
	B$_3$	149.3	20.0	0.99	17
MAO-3	**A$_1$**	110.4	15.7	0.30	43
	A$_2$	120.0	18.9	0.45	8
	B$_2$	125.5	17.0	0.45	13
	B$_1$	142.3	17.3	0.85	14
	D	153.0	20.7	0.80	7
	C	160.0	27.0	0.90	15

[a] From best fit of the ^{27}Al MAS NMR spectra for the experimental values. [b] In parentheses: averaged DFT-calculated values from **MAO-c-DFT** and **MAO-s-DFT**.

Experimental studies were performed on a commercial MAO sample, which was dried extensively under vacuum to remove excess and labile $AlMe_3$, affording a white solid (**MAO-1**). The ^{27}Al MAS NMR spectrum of **MAO-1** at 28.2 T and 50 kHz features signals ranging from approximately 160 to 60 ppm, with a maximum at 101 ppm (Figure 2d). Several discontinuities in the spectrum indicate the presence of overlapping sites. Similar to previously reported spectra,[21,22] this provides limited insight on its own. The MQMAS NMR sequence is ideally suited to decompose such complex, multicomponent spectra of a quadrupolar nucleus like ^{27}Al. By correlating chemical shift and quadrupolar interaction in a 2D acquisition mode, the individual components can be distinguished, although sensitivity for sites featuring high quadrupolar coupling constants

(C_Q) remains a challenge. In the present case, even with the ultrahigh magnetic field, and considering that sites with large C_Q values are expected to be present, we resorted to a specific sequence to enhance excitation of such sites, namely DFS-coslp-MQMAS.[30,31] The corresponding 2D spectrum resolves five main sites in **MAO-1** (Figure 2e). NMR parameters and relative ratios of these sites were extracted through simultaneous best-fit simulations of the MAS and DFS-coslp-MQMAS NMR spectra and confirmed by recording the data at a lower magnetic field of 19.97 T (Table 1, Figures 2d, S2, S3 and S4).[32] Comparison with DFT-calculated parameters allows for the assignment of spectral features. The main signal, accounting for about 40% of the Al environments, appears at 110.9 ppm with C_Q = 15.7 MHz, accounting for the **A$_1$** sites. The **B$_2$-C** framework gives rise to two sites, each corresponding to about 20% of the Al nuclei. These sites exhibit CS and C_Q of 124.0 ppm and 19.0 MHz, and 162.4 ppm and 27.4 MHz, respectively. The latter site is particularly remarkable due to its high CS and C_Q, in line with its unique structure and bonding characteristics. The **B$_1$** site signal is observed at a CS of 146.8 ppm with C_Q = 18.5 MHz, corresponding to approximately 10% of the Al centers. Finally, the **A$_2$** sites partially overlap with the **B$_2$** sites due to their similar NMR parameters (Table 1), making up about 5% of the total Al content.

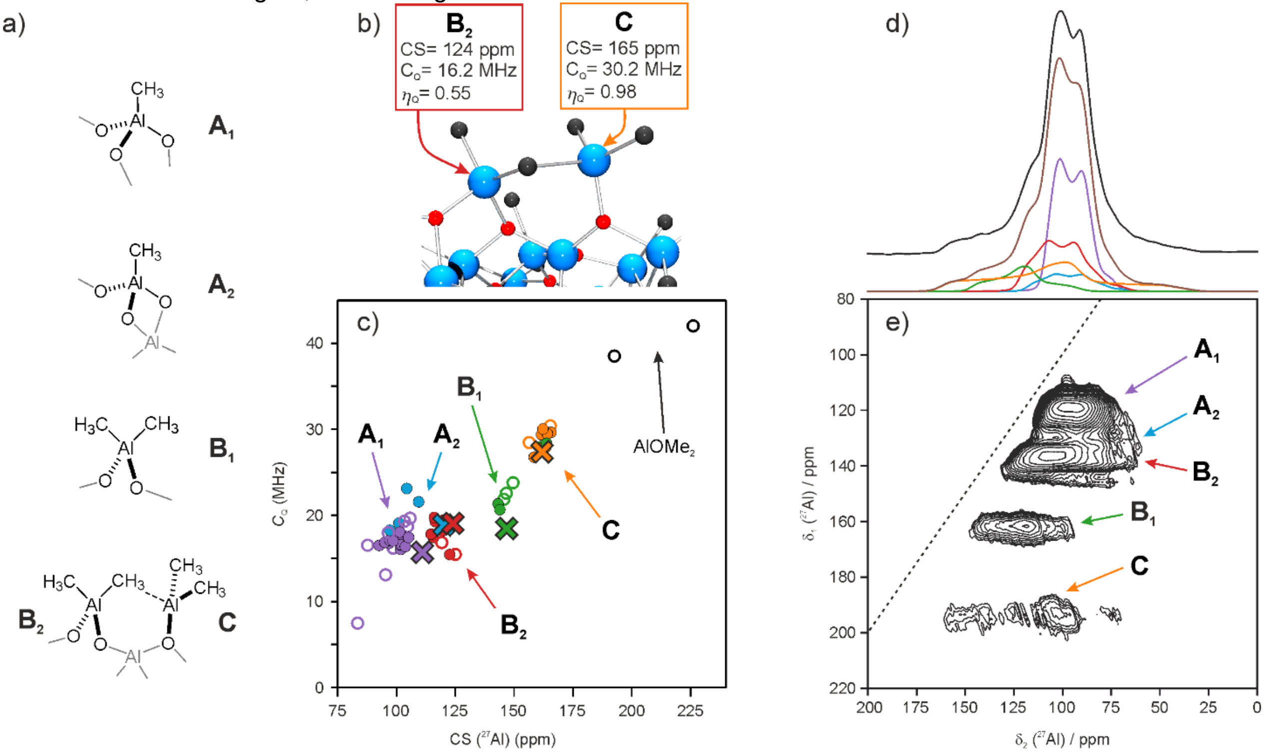

Figure 2. a) Main aluminum sites observed in MAO. Experimental and theoretical data for MAO: b) A representative **B$_2$-C** site from the **MAO-c-DFT** structure showing DFT-calculated ^{27}Al NMR parameters, H atoms omitted for clarity; c) Comparison of experimental and DFT-calculated chemical shift (CS) and C_Q values for **MAO-1** (✕), **MAO-c-DFT** (○) and **MAO-s-DFT** (●); The color code of the calculated points designates the nature of each site; d) ^{27}Al MAS NMR spectrum of **MAO-1** (28.2 T, spinning speed 50 kHz) along with the best fit based on MQ MAS data; The color code of the individual best-fit lines designates the nature of the site; e) ^{27}Al DFS-coslp-MQMAS NMR spectrum of **MAO-1** (28.2 T, spinning speed 50 kHz).

Therefore, this work provides a detailed view of this material's main structural features. The strong agreement between DFT-calculated and experimental NMR parameters supports the reliability of the assignments, demonstrating that ^{27}Al MAS NMR at ultra-high field (28.2 T) is a powerful tool for characterizing MAO.

Investigation of THF Reactivity Towards MAO

Lewis bases such as tetrahydrofuran (THF) are known to react with MAO, forming $AlMe_3$ adducts or adducts of the activating cation $[AlMe_2]^+$.[33,34] However, the impact of this reaction on the core structure of MAO remains unknown, making ^{27}Al MAS NMR an invaluable tool for investigation. The reactivity of **MAO-1** towards THF was probed through a gas phase reaction with THF at room temperature, followed by exposure to vacuum. This process yielded **MAO-2**, which was subsequently characterized by high-field multinuclear NMR. The ^{1}H MAS NMR spectrum at 28.2 T, in the AlMe region, features a broad major signal at about -0.9 ppm, along with a sharp peak at -1.06 ppm, with an intensity ratio of 5.7:1 (Figure 3a). The protons accounting to both signals are in close proximity to that of bound THF, as evidenced by ^{1}H-^{1}H DQSQ MAS NMR (Figure 3b). In line with previous reports,[33] the sharp peak at -1.06 ppm is attributed to [AlMe$_3$(THF)], a species arising from the extraction of AlMe$_3$ from TMA-depleted MAO. Given the overall AlMe$_n$ stoichiometry, this means that the TMA adduct represents about 8% of total aluminum. Furthermore, the THF/AlMe molar ratio, estimated to be 1:4 based on the integration of the ^{1}H MAS spectrum, suggests that a significant fraction of the THF molecules are bound to MAO, forming Lewis acid-base adducts. The nature of these sites was further explored by ^{27}Al NMR.

The ^{27}Al MAS NMR spectrum of **MAO-2** (Figure 3c) features signals ranging from 165 to 50, with several discontinuities and two maxima at 101 and 91 ppm. Compared with the spectrum of **MAO-1**, the intensity of the high-frequency signal at about 160 ppm is significantly reduced, indicating that THF coordination induces major changes. The presence of [AlMe$_3$(THF)] is evidenced by a characteristic low-field discontinuity around 171 ppm, in line with DFT calculated parameters, namely CS, C_Q and η_Q of 195 ppm, 32.9 MHz and 0.06, respectively (See Figure S5).[35] The ^{27}Al DFS-coslp-MQMAS NMR spectrum of **MAO-2** reveals five main sites (Figures 3d, S6 and S7). The signal from [AlMe$_3$(THF)] was not detected, due to both the low proportion of sites and extremely large quadrupolar coupling. Compared to **MAO-1**, the **A$_1$**, **A$_2$** and **B$_1$** sites are only slightly affected by THF coordination. However, the **B$_2$** and **C** sites, present in **MAO-1**, are no longer detected, and a new signal, labeled **B$_3$**, is observed at 152.2 ppm, with a C_Q of 20.0 MHz and a η_Q of 0.96. In addition, the **A$_1$** site overlaps with another newly formed component, **A$_3$**, which is more distinctly observed at lower magnetic fields (Fig. S8). Compared with **A$_1$**, this site exhibits a close chemical shift of 109.0 ppm, along with a larger C_Q and η_Q (16.5 MHz and 0.90).

These observations indicate the formation of two types of species upon THF addition to MAO. Following Path A in Figure 3e, the **B$_3$** sites originate from the coordination of THF onto the **C**-type aluminum centers, generating [-OAlMe$_2$(THF)] sites via cleavage of the Al-C bond with the bridging methyl group. DFT calculated NMR parameters are close to the experimental values (Figure 3f), supporting this assignment. This species may act as an intermediate in the generation of the [AlMe$_2$(THF)$_2$]$^+$ cation. However, as already reported in the literature[12] and suggested by ^{1}H NMR data, this cation is not efficiently extracted from MAO by THF alone and would require chelating Lewis bases such as bipyridine, for instance. This process generates **B$_1$** sites, which is confirmed by their increased relative proportion (from 9% in **MAO-1** to 19% in **MAO-2**).

The new sites, **A$_3$**, result from the attack of THF on **B$_2$** centers, yielding [O$_2$AlMe(THF)] centers and releasing the bridging methyl groups (Path B in Figure 3e). DFT calculations of NMR parameters (Figure 3g) indicate that **A$_3$** and **A$_1$** sites feature similar chemical shifts, but the former display higher C_Q, in agreement with experimental data. This reaction also generates [OAlMe$_3$] moieties from **C** sites, which subsequently coordinate with THF to release the [AlMe$_3$(THF)] species detected in the ^{1}H NMR spectrum. Notably, no signal corresponding to a [OAlMe$_3$] TMA adduct is detected, based on DFT calculated NMR parameters (CS, C_Q and η_Q of 165.5 ppm, 22.5 MHz and 0.08, respectively) (Figure S9). This dual reactivity of MAO towards a Lewis base is in line with previous EPR studies, which identified two types of Lewis-acidic centers using TEMPO radical as a Lewis base.[36] The present study demonstrates that ultra-high field ^{27}Al NMR enables a detailed molecular-level understanding of MAO's evolution upon Lewis base coordination.

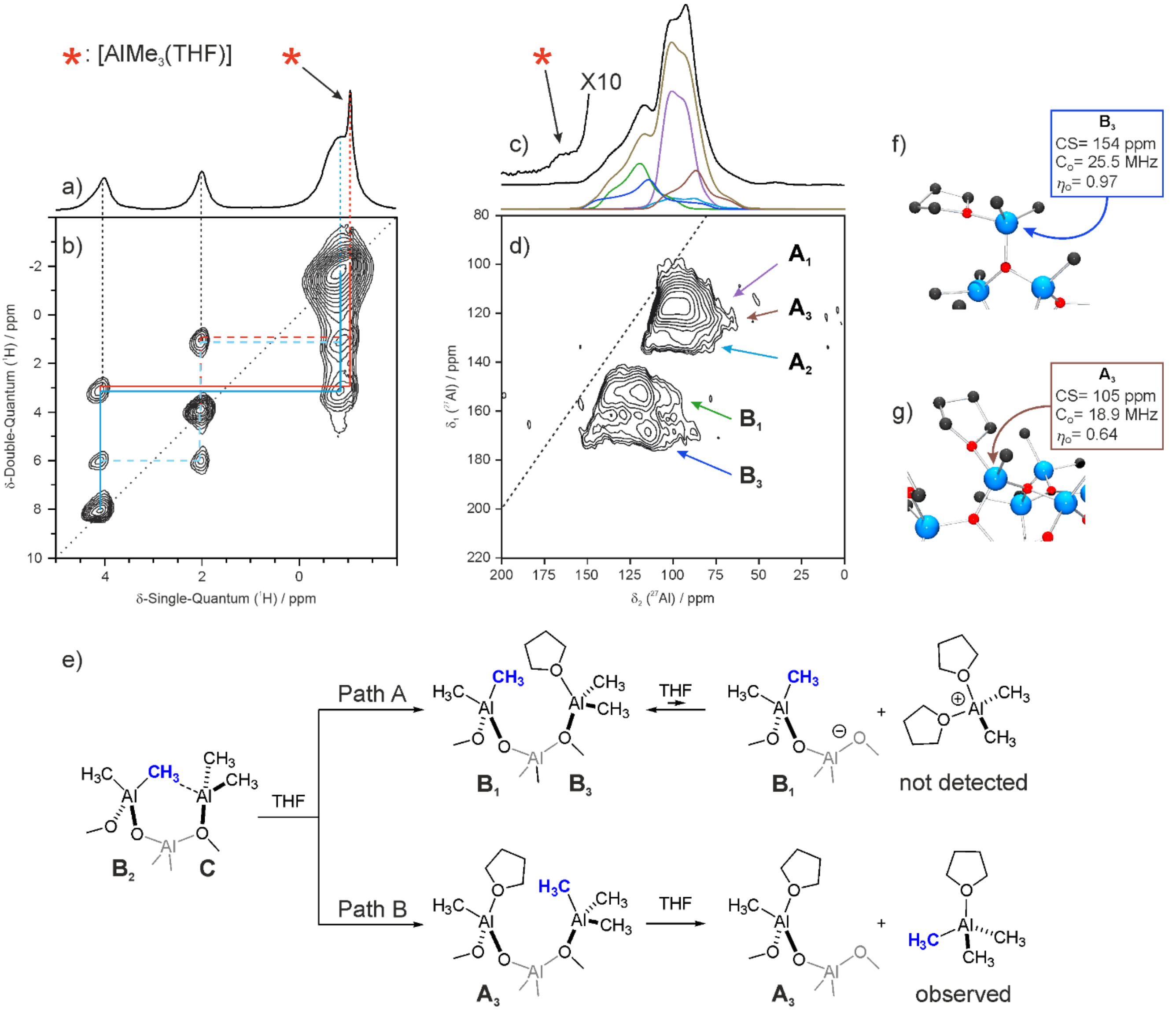

Figure 3. NMR characterization of **MAO-2** (28.2 T, spinning speed 50 kHz): a) ^{1}H MAS and b) ^{1}H-^{1}H DQSQ MAS NMR, c) ^{27}Al MAS NMR and best-fit simulation and d) ^{27}Al DFS-coslp-MQMAS NMR; e) Proposed pathways for THF interaction with **B$_2$**-**C** sites; f) DFT-calculated structure and NMR parameters of **B$_3$** sites; g) DFT-calculated structure and NMR parameters of **A$_3$** sites (H-atoms omitted for clarity).

Investigations on [ZrCp$_2$Me$_2$] Reactivity Towards MAO

To gain deeper understanding of MAO's ability to activate group 4 metallocenes, **MAO-1** was reacted with [ZrCp$_2$Me$_2$], in a Zr/Al molar ratio of 1/10, forming **MAO-3**. Although such a ratio is significantly higher than that of catalytically relevant systems, it still allows for structural analysis using ^{27}Al NMR. Given that the **B$_2$** and **C** sites each account for 20-25% of the Al content of **MAO-1**, the expected impact on spectroscopic features should be significant. Previous solution NMR [18,19] and IR [37] studies have suggested that under such conditions, the main species formed is the [MAO-ZrCp$_2$Me$_2$] adduct (of yet uncharacterized structure), with smaller amounts of [(ZrCp$_2$Me)$_2$-μ-Me][MeMAO] ion pairs.

While ^{1}H MAS NMR provides limited information, the ^{1}H-^{1}H DQSQ MAS NMR spectrum enables the identification of these two expected species, as evidenced by cross-peaks associating Cp and Me protons (Figure S10). The Zr-Me groups from the [MAO-ZrCp$_2$Me$_2$] adduct resonate at approximately -0.75 ppm, whereas those of [(ZrCp$_2$Me)$_2$-μ-Me][MeMAO] appear at around 0.3 (terminal ZrMe) and -0.8 ppm (bridging Me), in good agreement with solution NMR data (0.28 and -0.76 ppm, respectively[38,39]). In the case of the zirconocene adduct, the high-field position of the ZrMe signal, which resonates at a chemical shift very close to that of the AlMe protons (-0.70 ppm), suggests fast exchange between ZrMe and AlMe. The ^{13}C CP MAS

NMR spectrum features a broad signal ranging from 50 to -20 ppm, consistent with rapid exchange (on the NMR timescale) between Zr-Me and Al-Me groups (Figure S11). These elements are fully in line with previous DFT calculations on the exchange process within a model MAO-[$ZrCp_2Me_2$] adduct.[40] This is further supported by the ^1H MAS NMR data obtained at a higher Zr/Al ratio (1/2, **MAO-4**, Figure S14), where ZrMe protons resonate at -0.36 ppm (for comparison, [$ZrCp_2Me_2$] gives rise to a signal at -0.13 ppm). The shift towards higher CS values, compared to **MAO-3**, is in line with a shift of the equilibrium between free and MAO-interacting $ZrCp_2Me_2$, favoring the free zirconocene species.

The ^{27}Al NMR data align with the expected moderate changes upon addition of the dimethylzirconocene, remaining close to that of **MAO-1** (Figure 4a). The ^{27}Al DFS-coslp-MQMAS NMR spectrum (Figure 4b, S12, S13) reveals an additional signal with a CS of 153.0 ppm and a C_Q of 20.7 MHz, labelled as site **D**. Subtle changes within the MAO framework are evidenced in the comparison of projections from the anisotropic dimension of the DFS-coslp-MQMAS NMR spectra of **MAO-1**, **MAO-3** and **MAO-4** (Figure 4c). With increasing Zr/Al ratio, the proportion of **C** and **B$_2$** sites decreases, while the share of **D** and **B$_1$** sites increases. Interestingly, **B$_1$** centers shift towards lower CS and C_Q values, indicating perturbation of their environment. A similar trend is observed for **C** sites, which persist (though in low quantities) in **MAO-4**. This indicates that not all **B$_2$-C** frameworks display the same reactivity, as some are still observed even in the presence of excess dimethylzirconocene.

Based on previous theoretical investigations[41] and our experimental data, we propose that the zirconocene adduct forms upon reaction with **B$_2$-C** sites. This leads to the formation of **B$_1$** sites, along with a species where formerly **C** sites (coordinatively unsaturated [$O\text{-}AlMe_2$]) interact with [$ZrCp_2Me_2$] through a methyl bridge (**Figure 4**), generating [$O\text{-}AlMe_2\text{-}\mu\text{-}Me\text{-}ZrCp_2Me$], assigned to site **D**. Remarkably, the present DFT calculations of NMR parameters for site **D** closely match the experimental data, strongly supporting this assignment and the postulated reaction pathway.

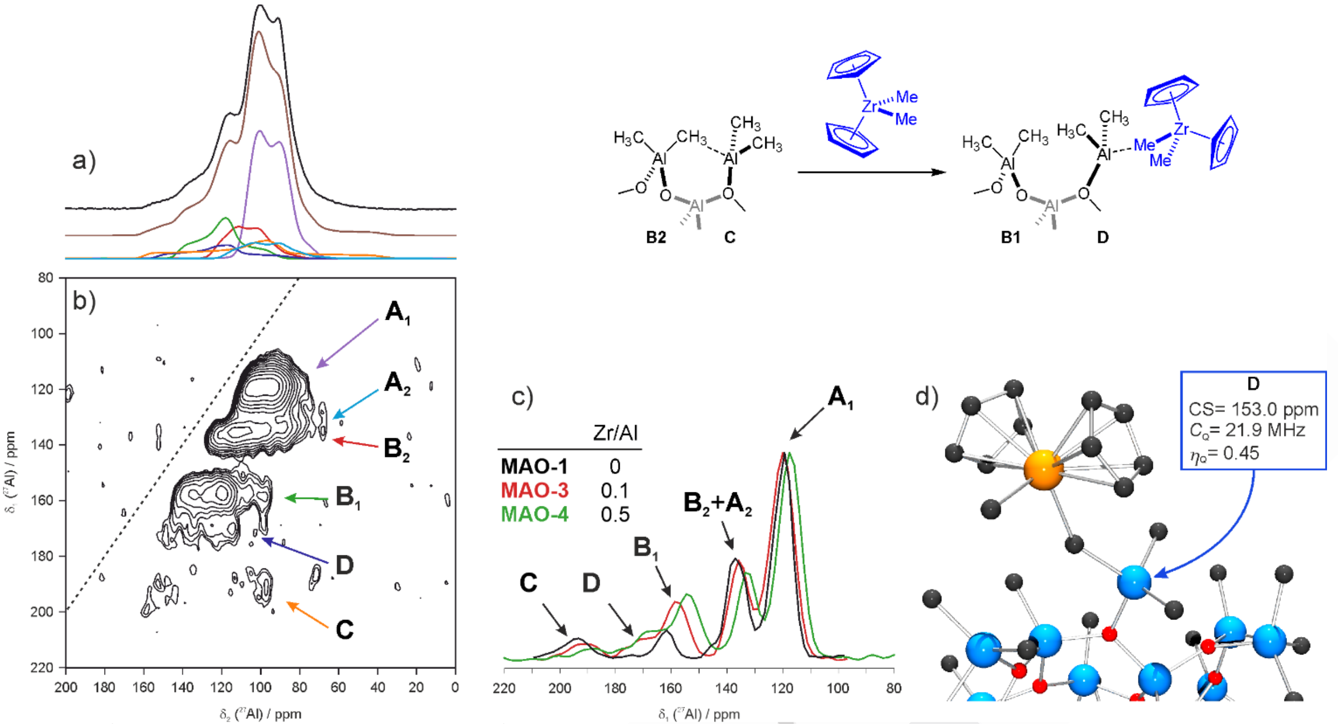

Figure 4. a) ^{27}Al MAS NMR (with best-fit simulation) and b) ^{27}Al DFS-coslp-MQMAS NMR spectra of **MAO-3** (28.2 T, spinning speed 50 kHz); c) Projections from the anisotropic dimension of the ^{27}Al MQMAS NMR spectra of **MAO-1** (black trace), **MAO-3** (red trace) and **MAO-4** (green trace); d) DFT-calculated representation of site **D,** along with DFT-calculated NMR parameters. H atoms omitted for clarity.

Conclusion

This study features the first detailed experimental insights by NMR into the molecular structure of MAO, a key component of the polyolefin industry that has long been the subject of on-going debate. Thanks to ultra-high magnetic field and high spinning frequency coupled with state-of-the-art NMR methods and DFT calculations, a detailed structural analysis of key motifs in MAO has been possible. This work helps in providing a clearer view on the structure and reactivity of MAO. Most saliently, we have presented a precise perspective on MAO's reactivity towards a Lewis base, unfolding a complex reaction scheme which has remained inaccessible to experimental studies until now. In the context of olefin polymerization catalysis, unprecedented spectroscopic evidence has been provided for the formation pathway and structure of a zirconocene-MAO adduct, representing the first step in precatalyst activation by MAO. This approach paves the way for numerous future investigations, including on the understanding of the initiation of MAO-metallocene-based polymerization systems. The complex chemistry of MAO and its critical role in catalytic processes provide challenging questions, ones that we intend to tackle through this combined experimental and theoretical methodology.

Supporting Information

Experimental details, additional spectroscopic data, atomic coordinates for the DFT optimized structures and relevant references. The authors have cited additional references within the Supporting Information.[42-44]

Acknowledgements

Chevreul Institute (FR 2638), Ministère de l'Enseignement Supérieur, de la Recherche et de l'Innovation, Hauts-de-France Region, and FEDER are acknowledged for supporting and partially funding this work. ChimieParisTech–PSL, CPE-Lyon and CNRS are thanked for financial support. Financial support from the IR INFRANALYTICS FR2054 for conducting the research is gratefully acknowledged. JA acknowledges support for the theoretical component of this research by the National Science Foundation grant CHE-2152633.

Keywords: solid state NMR • aluminum • polyolefins • structure elucidation • DFT calculations

[1] M. J. Krause, F. Orlandi, A. T. Saurage, J. R. Zietz, *Aluminum Compounds, Organic* in *Ullmann's Encyclopedia of Industrial Chemistry*, Vol. 2, Wiley-VCH, Weinheim, **2012**, pp. 586-605.

[2] W. Kaminsky, "Discovery of Methylaluminoxane as Cocatalyst for Olefin Polymerization"*Macromolecules*, **2012**, *45*, 3289-3297.

[3] H. S. Zijlstra, S. Harder, “Methylalumoxane – History, Production, Properties, and Applications” *Eur. J. Inorg. Chem.* **2015**, 19–43.

[4] T. K. Trefz, M. A. Henderson, M. Y. Wang, S. Collins, J. S. McIndoe, “Mass Spectrometric Characterization of Methylaluminoxane” *Organometallics*, **2013**, *32*, 3149−3152.

[5] H. S. Zijlstra, M. Linnolahti, S. Collins, J. S. McIndoe, “Additive and Aging Effects on Methylalumoxane Oligomers” *Organometallics* **2017**, *36*, 1803−1809.

[6] M. R. Mason, J. M. Smith, S. G. Bott, A. R. Barron, “Hydrolysis of tri-tert-butylaluminum: the first structural characterization of alkylalumoxanes [(R$_2$Al)$_2$O]$_n$ and (RAlO)$_n$” *J. Am. Chem. Soc.* **1993**, *115*, 4971-4984.

[7] M. Watanabi, C. N. McMahon, C. J. Harlan, A. R. Barron “Reaction of Trimethylaluminum with [(^{t}Bu)Al(μ_3-O)]$_6$: Hybrid *tert*-Butylmethylalumoxanes as Cocatalysts for Olefin Polymerization” *Organometallics* **2001**, *20*, 460-467.

[8] E. Zurek, T. Ziegler, “Theoretical studies of the structure and function of MAO (methylaluminoxane)” *Prog. Polym. Sci.* **2004**, *29*, 107–148.

[9] M. Linnolahti, J. R. Severn, T. A. Pakkanen, “Are Aluminoxanes Nanotubular? Structural Evidence from a Quantum Chemical Study” *Angew. Chem. Int. Ed.* **2006**, *45*, 3331-3334.

[10] Z. Falls, N. Tymińska, E. Zurek, “The Dynamic Equilibrium Between (AlOMe)$_n$ Cages and (AlOMe)$_n$·(AlMe$_3$)$_m$ Nanotubes in Methylaluminoxane (MAO): A First-Principles Investigation” *Macromolecules*, **2014**, *47*, 8556-8569.

[11] M. Linnolahti, S. Collins, “Formation, Structure, and Composition of Methylaluminoxane” *ChemPhysChem* **2017**, *18*, 3369 – 3374.

[12] F. Ghiotto, C. Pateraki, J. Tanskanen, J. R. Severn, N. Lühmann, A. Kusmin, J. Stellbrink, M. Linnolahti, M. Bochmann, “Probing the Structure of Methylalumoxane (MAO) by a Combined Chemical, Spectroscopic, Neutron Scattering, and Computational Approach” *Organometallics*, **2013**, *32*, 3354 – 3362.

[13] L. Luo, S. A. Sangokoya, X. Wu, S. P. Diefenbach, B. Kneale (Albemarle Corporation), U. S. Pat. Appl., 0062492A1, **2009**.

[14] V. Busico, R. Cipullo, F. Cutillo, N. Friederichs, S. Ronca, B. Wang, “Improving the Performance of Methylalumoxane: A Facile and Efficient Method to Trap “Free” Trimethylaluminum” *J. Am. Chem. Soc.* **2003**,*125*,12402–12403.

[15] F. Zaccaria, P. H. M. Budzelaar, R. Cipullo, C. Zuccaccia, A. Macchioni, V. Busico, C. Ehm, “Reactivity Trends of Lewis Acidic Sites in Methylaluminoxane and Some of Its Modifications” *Inorg. Chem.* **2020**, *59*, 5751−5759.

[16] L. Luo, J. M. Younker, A. V. Zabula, “Structure of methylaluminoxane (MAO): Extractable [Al(CH$_3$)$_2$]$^+$ for precatalyst activation” *Science*, **2024**, *383*, 1424-1428.

[17] C. J. Harlan, S. G. Bott, A. R. Barron, “Three-Coordinate Aluminum Is Not a Prerequisite for Catalytic Activity in the Zirconocene-Alumoxane Polymerization of Ethylene” *J. Am. Chem. Soc.* **1995**, *117*, 6465–6474.

[18] I. Tritto, R. Donetti, M. C. Sacchi, P. Locatelli, G. Zannoni, “Dimethylzirconocene−Methylaluminoxane Catalyst for Olefin Polymerization: NMR Study of Reaction Equilibria” *Macromolecules*, **1997**, *30*, 1247-1252.

[19] D. E. Babushkin, N. V. Semikolenova, V. A. Zakharov, E. P. Talsi, “Mechanism of dimethylzirconocene activation with methylaluminoxane: NMR monitoring of intermediates at high Al/Zr ratios” *Macromol. Chem. Phys.* **2000**, *201*, 558–567.

[20] Z. Falls, E. Zurek, J. Autschbach, “Computational prediction and analysis of the ^{27}Al solid-state NMR spectrum of methylaluminoxane (MAO) at variable temperatures and field strengths” *Phys. Chem. Chem. Phys.* **2016**, *18*, 24106-24118.

[21] P. L. Bryant, C. R. Harwell, A. A. Mrse, E. F. Emery, Z. Gan, T. Caldwell, A. P. Reyes, P. Kuhns, D. W. Hoyt, L. S. Simeral, R. W. Hall, L. G. Butler, “Structural Characterization of MAO and Related Aluminum Complexes. 1. Solid-State ^{27}Al NMR with Comparison to EFG Tensors from ab Initio Molecular Orbital Calculations” *J. Am. Chem. Soc.* **2001,** *123,* 12009-12017.

[22] M. A. Bashir, T. Vancompernolle, R. M. Gauvin, L. Delevoye, V. Monteil, M. Taoufik, T. F. L. McKenna, C. Boisson, “Silica/MAO/(*n*-BuCp)$_2$ZrCl$_2$ catalyst: effect of support dehydroxylation temperature on the grafting of MAO and ethylene polymerization“ *Cat. Sci. Tech.*, **2016**, *6*, 2962-2974.

[23] F.-J. Wu, L. S. Simeral, A. A. Mrse, J. L. Eilertsen, L. Negureanu, Z. Gan, F. R. Fronczek, R. W. Hall, L. G. Butler, “Structural Characterization of Al$_{10}$O$_6$^{i}Bu$_{16}$(μ-H)$_2$, a High Aluminum Content Cluster: Further Studies of Methylaluminoxane (MAO) and Related Aluminum Complexes” *Inorg. Chem.* **2007**, *46*, 44-47.

[24] S. K. Wolff, T. Ziegler, E. van Lenthe, E. J. Baerends, “Density functional calculations of nuclear magnetic shieldings using the zeroth-order regular approximation (ZORA) for relativistic effects: ZORA nuclear magnetic resonance” *J. Chem. Phys.* **1999**, *110*, 7689–7698.

[25] J. Autschbach, E. Zurek, “Relativistic Density-Functional Computations of the Chemical Shift of ^{129}Xe in Xe@C$_{60}$” *J. Phys. Chem. A* **2003**, *107*, 4967-4972.

[26] E. J. Baerends, N. F. Aguirre, N. D. Austin, J. Autschbach, F. M. Bickelhaupt, R. Bulo, C. Cappelli, A. C. T. van Duin, F. Egidi, C. Fonseca Guerra, A. Förster, M. Franchini, T. P. M. Goumans, T. Heine, M. Hellström, C. R. Jacob, L. Jensen, M. Krykunov, E. van Lenthe, A. Michalak, M. M. Mitoraj, J. Neugebauer, V. Paul Nicu, P. Philipsen, H.

Ramanantoanina, R. Rüger, G. Schreckenbach, M. Stener, M. Swart, J. M. Thijssen, T. Trnka, L. Visscher, A. Yakovlev, S. van Gisbergen, "The Amsterdam Modeling Suite" *J. Chem. Phys.* **2025**, *162*, 162501

[27] J. P. Perdew, K. Burke, M. Ernzerhof, "Generalized Gradient Approximation Made Simple"

[28] B. Hammer, L. B. Hansen, J. K. Norskov, "Improved Adsorption Energetics within Density-Functional Theory Using Revised Perdew-Burke-Ernzerhof Functionals" *Phys. Rev. B* **1999**, 59, 7413-7421.

[29] The influence of a bridging methyl group on an Al environment's CS and C_Q is observed in one of the two $[OAlMe_2]$ sites, showing calculated values of 193 ppm for CS and about 38.6 MHz for C_Q. In this case, the interaction with the bridging methyl group from a neighboring $[O_3AlMe]$ group is less pronounced, as indicated by the Al-C distance of 2.608 Å and the sum of the bond angles around the aluminum of 356.8°, compared to the interaction with the $[O_2AlMe_2]$ counterparts. Consequently, the Al environment within this $[AlO_3Me]$ moiety features comparatively lower CS and C_Q values than the non-interacting $[AlO_3Me]$ sites (84 ppm and 7.4 MHz).

[30] I. Hung, Z. Gan, "On the use of single-frequency versus double-frequency satellite-transition pulses for MQMAS" *J. Magn. Reson.* **2021**, *328*, 106994.

[31] A. Sasaki, J. Trébosc, H. Nagashima, J.-P. Amoureux, "On the applicability of cosine-modulated pulses for high-resolution solid-state NMR of quadrupolar nuclei with spin > 3/2" *Solid State Nucl. Magn. Reson.*, **2023**,*125*, 101863.

[32] NMR parameters of the first 3 sites were confirmed by comparison with data acquired on a 19.97 T spectrometer, while the importance of using the DFS-coslp-MQMAS NMR sequence is demonstrated by comparison to classical MQ MAS pulse sequences such as z-filter or FAM (Fig S4).

[33] D. W. Imhoff, L. S. Simeral, S. A. Sangokoya, J. H. Peel, J. H. "Characterization of Methylaluminoxanes and Determination of Trimethylaluminum Using Proton NMR" *Organometallics* **1998**, *17*, 1941-1945.

[34] H. S. Zijlstra, A. Joshi, M. Linnolahti, S. Collins, J. Scott McIndoe, "Interaction of Neutral Donors with Methylaluminoxane" *Eur. J. Inorg. Chem.* **2019**, 2346-2355.

[35] R. Behn, E. Janssen, H. Lehmkuhl, A. Rufinska,"^{27}Al-NMR Spektroskopie zur Charakterisierung von Organoaluminium-Verbindungen" *J. Organomet. Chem.*, **1987**, *333*, 155-168.

[36] E.P. Talsi, N.V. Semikolenova, V.N. Panchenko, A.P. Sobolev, D.E. Babushkin, A.A. Shubin, V.A. Zakharov, "The metallocene/methylaluminoxane catalysts formation: EPR spin probe study of Lewis acidic sites of methylaluminoxane" *J. Mol. Catal. A: Chem.*, **1999**, *139*, 131–137.

[37] J. L. Eilertsen, J. A. Støvneng, M. Ystenes, E. Rytter, "Activation of Metallocenes for Olefin Polymerization As Monitored by IR Spectroscopy" *Inorg. Chem.* **2005**, *44*, 4843-4851.

[38] M. Bochmann, S. J. Lancaster, "Monomer–Dimer Equilibria in Homo- and Heterodinuclear Cationic Alkylzirconium Complexes and Their Role in Polymerization Catalysis" *Angew. Chem. Int. Ed.* **1994**, *33*, 1634-1637.

[39] R. A. Petros, J. R. Norton, "Effectiveness in Catalyzing Carboalumination Can Be Inferred from the Rate of Dissociation of M/Al Dimers" *Organometallics* **2004**, *23*, 5105–5107.

[40] E. Zurek, T. Ziegler, "Toward the Identification of Dormant and Active Species in MAO (Methylaluminoxane)-Activated, Dimethylzirconocene-Catalyzed Olefin Polymerization" *Organometallics* **2002**, *21*, 83-92.

[41] S. Collins, M. Linnolahti, "Activation of Substituted Metallocene Catalysts Using Methylaluminoxane" *ChemCatChem* **2022**, *14*, e202101918.

[42] M. Carravetta, M. Eden, X. Zhao, A. Brinkmann, M. H. Levitt, "Symmetry principles for the design of radiofrequency pulse sequences in the nuclear magnetic resonance of rotating solids" *Chem. Phys. Lett.* **2000**, *321*, 205-215.

[43] L. Mafra, R. Siegel, C. Fernandez, D. Schneider, F. Aussenac, J. Rocha, "High-resolution ^{1}H homonuclear dipolar recoupling NMR spectra of biological solids at MAS rates up to 67 kHz" *J. Magn. Reson.* **2009**, *199*, 111–114.

[44] S. G. J. van Meerten, W. M. J. Franssen, A. P. M. Kentgens, "ssNake: A cross-platform open-source NMR data processing and fitting application" *J. Magn. Reson.* **2019**, *301*, 56–66.

.

10.1002/anie.202508409

Entry for the Table of Contents

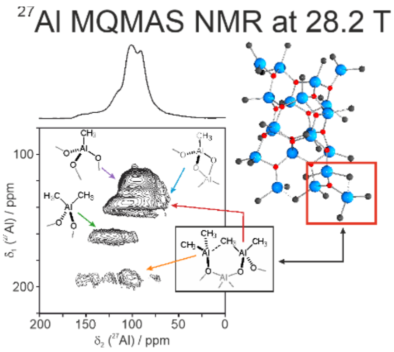

The molecular structure of olefin polymerization activator methylaluminoxane (MAO) was probed using ultra-high field solid-state NMR backed with DFT calculations, revealing its key motifs and reactive centers.